• Article •

Spinodal dynamics of metastable glass transition domains in amorphous polymer towards thermomechanically tailorable shape memory effect

LIU JingYun [1], LU HaiBao[1*] & FU Yong-Qing [2*]

[1] *Science and Technology on Advanced Composites in Special Environments Laboratory, Harbin Institute of Technology, Harbin 150080, China;*
[2] *Faculty of Engineering and Environment, Northumbria University, Newcastle upon Tyne, NE1 8ST, UK*

Received April 21, 2015, accepted July 1, 2015; published online August 25, 2015

Glass transition plays a critical role to determine the dynamic behaviors of amorphous shape memory polymers (SMPs). However, the fundamental relationships between shape memory effect (SME) and dynamic glass transition have not been well understood, even though this topic has been studied for decades. In this study, we apply a mean-square displacement function of Adam-Gibbs (AG) domain size model to explore metastable glass transition between normal glass state and rubbery state of amorphous SMPs, based on both mode-coupling theory and mean-field model. A statistic viscosity equation is formulated to study the dynamic glass transition of metastable AG domains in an amorphous SMP. A dynamically spinodal model is also developed to connect dynamic glass transitions to thermomechanical processes, based on statistic viscosity equation and phase transition model. Furthermore, using the spinodal models, multiple shape memory behaviors have been predicted for amorphous SMPs with dual-, triple- and quadruple-SMEs, resulted from their different routes of themomechanical evolutions. Finally, the proposed models are verified using the experimental data reported in literature.

shape memory polymer, glass transition, dynamics, metastable

Citation: Liu J Y, Lu H B, Fu Y Q. Spinodal dynamics of metastable glass transition domains in amorphous polymer towards thermomechanically tailorable shape memory effect. Sci China Tech Sci,

1 Introduction

Inspired by varieties of structures, functionalities, behaviors and interactions of organisms in nature, smart soft matters, which can sense and respond to the environmental changes [1], have been developed [2-7] to respond to external stimuli [8-13], possess highly designable properties [14-16], and achieve excellent biocompatibility [17]. These soft matters have found various practical applications in biomedical devices [18-21], flexible electronics [22,23], smart robotics [24] and space deployable structures [25,26]. Being one of the most popular smart soft matters, shape memory polymers (SMPs) have attracted extensive attention due to their distinguished characteristics of designable shape memory effect (SME) and tailorable shape recovery behaviors [27,28].

Glass transition is one of the key dynamic factors to determine the SME in an amorphous SMP, and it is mainly resulted from the strain energies being preserved and/or released by the molecular soft segments [29,30]. In the last three decades, many studies have attempted to formulate the fundamental relationship between SME and glass transition temperature (T_g) of the amorphous SMPs. For example, Li *et al*. [31] developed a constitutive model of glassy-rubbery phase transition to predict the dual-SME for the amorphous SMPs. Nguyen *et al*. [32] and Yu *et al*. [33] introduced multi-branch Maxwell models to analyze multi-SMEs in amorphous SMPs undergoing multi-stage glass transitions. Xie *et al*. [34] synthesized amorphous Nafion SMPs, which exhibited dual-, triple- and quadruple-SMEs, with wide plateau ranges of T_g. However, so far, there are few studies which have been conducted to explore spinodal dynamics in an amorphous SMP, of which the glass transition is governed by the non-equilibrium dynamics while can reveal the equilibrium of SME.

In this study, the Langevin process [35] in Adam-Gibbs (AG) domains [36] is employed to investigate metastable glass transitions in amorphous SMPs. A constitutive rela-

*Corresponding author (email: luhb@hit.edu.cn; richard.fu@northumbria.ac.uk)

tionship between the mean-square displacement and dynamic viscosity is firstly formulated to describe the AG domains undergoing their metastable glass transitions, based on the mode-coupling theory and mean-field model [37], as well as the scaling theory [38]. A dynamic spinodal model is then developed to explore the connection between thermomechanical process and glass transition of the metastable AG domains, based on the statistic viscosity equation and phase transition theory [39]. Furthermore, multiple shape memory behaviors have been studied using the dynamically spinodal model, which is verified using the experimental data reported in literature [34,40].

2 Theoretical framework

According to the AG domain size model [36] and scaling theory [38], glass transition is defined to present evolutions of spinodal regions in the amorphous polymer. As shown in Figure 1(a), there are three types of AG domains, i.e., meta stable glass state (in the spinodal region), normal glass state (below the spinodal curve) and rubbery state (above the spinodal curve). Figure 1(b) illustrates the molecular structures of these three types of AG domains. In Figure 1(c), the dynamic mean-square displacements are used to describe these AG domains, and constitutive relationships between mean-square displacement and relaxation time (τ) for these three cases have been plotted in this figure [41].

Dynamic equilibrium of the Langevin process is then employed to describe the mean-square displacement for amorphous polymers [35,42],

$$\frac{D^2}{2d^2}\left[m\frac{\mathrm{d}^2 r}{\mathrm{d}\tau^2}+\zeta\frac{\mathrm{d}r}{\mathrm{d}\tau}\right]=T-\frac{1}{T}\int_0^{\tau}\frac{\mathrm{d}r(u)}{\mathrm{d}\tau}M(\tau-u)\mathrm{d}u \quad (1)$$

where D is the initial mean-square displacement of the AG domain [37], d is the spatial dimensions, m is the mass of the AG domain [37], $r(\tau)$ is the mean-square displacement as a function of the relaxation time (τ) at T_g [37], ζ is the friction coefficient for relaxation of AG domain [35,42], $M(\tau)$ is the relaxation time function determined by the thermomechanical process of the AG domain [35,42], T is the temperature, and u is the integral variable of relaxation time.

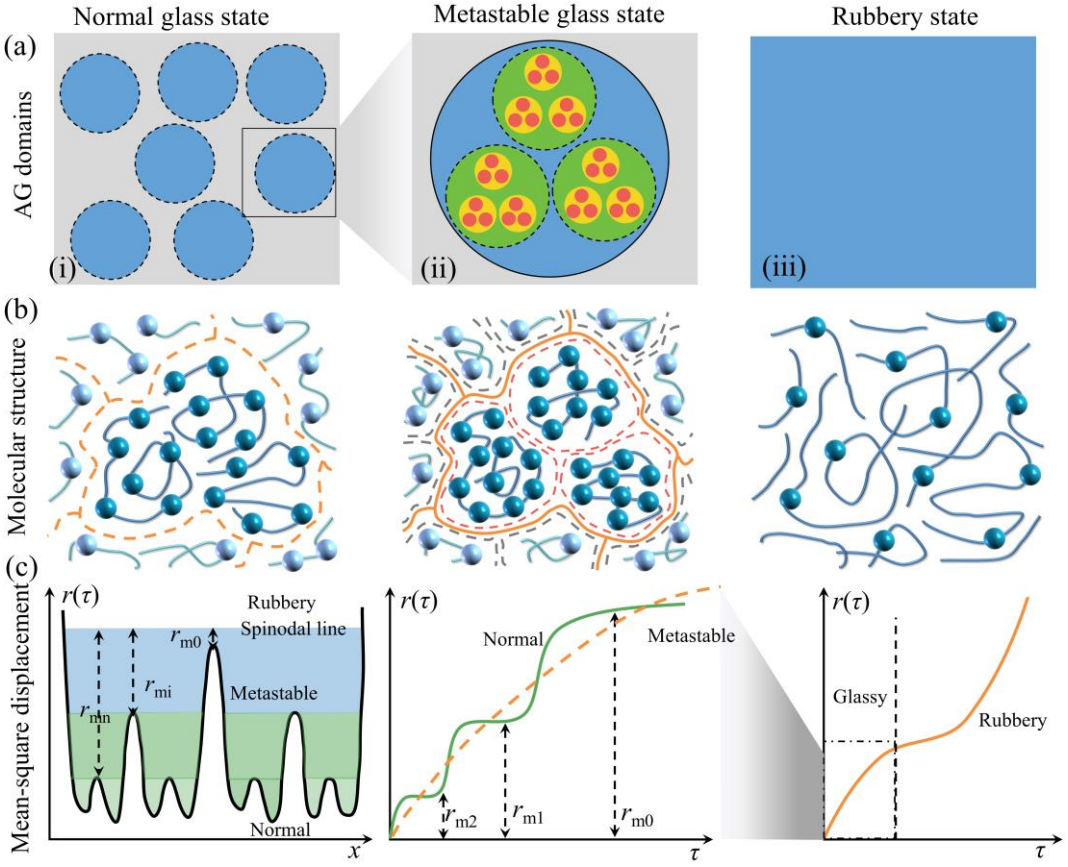

Figure 1 Schematic illustration of the metastable glass state, normal glass state and rubbery state in amorphous polymer, using three types of AG domains, respectively. (a) AG domains; (b) Molecular structures; (c) Effect of the mean-square displacement on the glass transition.

According to the mode-coupling theory, there is a constitutive relationship between the relaxation time ($M(\tau)$) and mean-square displacement ($r(\tau)$) at T_g [35],

$$M(\tau)=r^2(\tau) \tag{2}$$

Based on the mean-field model [35], the viscosity of amorphous polymer (η) can be obtained,

$$\eta=\frac{3\varphi}{TV_D}\int_0^{\infty}M(\tau)\mathrm{d}\tau \tag{3}$$

where $\varphi=\rho V_D$ is the weight fraction, V_D is the volume, and ρ is the density of the AG domain [35].

Equation (3) can be re-written as,

$$\eta=\frac{3\rho V_D}{TV_D}\int_0^{\infty}M(\tau)\mathrm{d}\tau=\frac{3\rho}{T}\int_0^{\infty}M(\tau)\mathrm{d}\tau \tag{4}$$

Substituting equation (2) into (4), the viscosity (η) can be expressed as a function of the mean-square displacement ($r(\tau)$) as,

$$\eta=\frac{3\rho}{T}\int_0^{\infty}M(\tau)\mathrm{d}\tau=\frac{3\rho}{T}\int_0^{\infty}r^2(\tau)\mathrm{d}\tau \tag{5}$$

The mean-square displacement can predict the existence of a dynamical glass transition, and $r(\tau)$ is a simple function of τ alone (essentially, $r(\tau)\sim\tau^2$) when the polymer segment only vibrates around the equilibrium position. Simultaneously, the mean-square displacement has another form of τ when the segment starts to relax and the glass transition starts to occur. Therefore, the mean-square displacement function ($r(\tau)$) can be written using the following equations [35-38],

$$r(\tau)=5\tau^2 \quad (0<\tau<\tau_{\mathrm{mn}}) \tag{6a}$$

$$r(\tau)=r_{\mathrm{mi}}-B\tau^{-b} \quad (\tau_{\mathrm{mi}}<\tau<\tau_{\mathrm{mi-1}},1\le i\le \mathrm{n}) \tag{6b}$$

where r_{mi} and τ_{mi} are the mean-square displacement and relaxation time of the ith plateau in glass transition region, respectively. B is a material constant [35,42], and b is an exponential constant [35,42].

Combining equations (5) and (6), the viscosity can be finally obtained as,

$$\eta=\frac{3\rho}{T}\int_0^{\tau}r^2(\tau)\mathrm{d}\tau=\begin{cases}\dfrac{3\rho}{T}\left[\displaystyle\int_0^{\tau_{\mathrm{mn}}}\left(5\tau^2\right)^2\mathrm{d}\tau+\sum_{i=1}^{i=\mathrm{n}}\int_{\tau_{\mathrm{di}}}^{\tau_{\mathrm{di-1}}}\left(r_{\mathrm{mi}}-B\tau^{-b}\right)^2\mathrm{d}\tau\right] & (0<\tau<\tau_{\mathrm{mn}})\\ \dfrac{3\rho}{T}\left[5\tau_{\mathrm{mn}}^5+\displaystyle\sum_{i=1}^{i=\mathrm{n}}\left(r_{\mathrm{mi}}^2t+2Br_{\mathrm{mi}}\frac{t^{-b+1}}{b-1}+B^2\frac{t^{-2b+1}}{-2b+1}\right)\Bigg|_{\tau_{\mathrm{mi}}}^{\tau_{\mathrm{mi-1}}}\right] & (\tau_{\mathrm{mi}}<\tau<\tau_{\mathrm{mi-1}},1\le i\le \mathrm{n})\end{cases} \tag{7}$$

where t is the integral variable of time.

Based on the phase transition theory [39] and equation (7), the relationship of the stored strain (ε_{s}) and pre-stored strain ($\varepsilon_{\mathrm{pre}}$) can be expressed by the viscosity (η) as,

$$\frac{\varepsilon_{\mathrm{s}}}{\varepsilon_{\mathrm{pre}}}=1-\frac{T}{3\rho}\Bigg/\left[5\tau_{\mathrm{mn}}^5+\sum_{i=1}^{i=\mathrm{n}}\left(r_{\mathrm{mi}}^2t+2Br_{\mathrm{mi}}\frac{t^{-b+1}}{b-1}+B^2\frac{t^{-2b+1}}{-2b+1}\right)\Bigg|_{\tau_{\mathrm{mi}}}^{\tau_{\mathrm{mi-1}}}\right] \tag{8}$$

where $\varepsilon_{\mathrm{s}}=\varepsilon-\varepsilon_0$ (ε is the total strain and ε_0 is the initial strain). The total strain (ε) can be expressed as,

$$\varepsilon=\varepsilon_0+\varepsilon_{\mathrm{s}}=\varepsilon_0+\varepsilon_{\mathrm{pre}}\frac{\varepsilon_{\mathrm{s}}}{\varepsilon_{\mathrm{pre}}}=\varepsilon_0+\varepsilon_{\mathrm{pre}}-\frac{\varepsilon_{\mathrm{pre}}T}{3\rho}\Bigg/\left[5\tau_{\mathrm{mn}}^5+\sum_{i=1}^{i=\mathrm{n}}\left(r_{\mathrm{mi}}^2t+2Br_{\mathrm{mi}}\frac{t^{-b+1}}{b-1}+B^2\frac{t^{-2b+1}}{-2b+1}\right)\Bigg|_{\tau_{\mathrm{mi}}}^{\tau_{\mathrm{mi-1}}}\right] \tag{9}$$

According to the phase transition theory [39], the strain will be released from the deformed strain $\varepsilon_{\mathrm{load},j}$ to stored strain $\varepsilon_{\mathrm{sj}}$, and the strain can therefore be expressed as,

$$\begin{aligned}\varepsilon&=\varepsilon_{sj}+(\varepsilon_{\mathrm{load},j}-\varepsilon_{sj})\frac{\varepsilon-\varepsilon_{sj}}{\varepsilon_{\mathrm{load},j}-\varepsilon_{sj}}, \qquad \text{(shape fixation)}\\ &=\varepsilon_{sj}+(\varepsilon_{\mathrm{load},j}-\varepsilon_{sj})\left[1-\frac{T}{3\rho}\Bigg/\left(5\tau_{\mathrm{mn}}^5+r_{\mathrm{mn}}^2t+2Br_{\mathrm{mn}}\frac{t^{-b+1}}{b-1}+B^2\frac{t^{-2b+1}}{-2b+1}\right)\right]\end{aligned} \tag{10a}$$

$$\varepsilon=\varepsilon_{sj-1}+\varepsilon_{\mathrm{pre},j}\frac{\varepsilon_{\mathrm{s}}}{\varepsilon_{\mathrm{pre},j}}=\varepsilon_{sj-1}+\varepsilon_{\mathrm{pre},j} \qquad \text{(shape recovery)}$$

$$-\frac{\varepsilon_{\mathrm{pre},j}T}{3\rho}\Bigg/\left[5\tau_{\mathrm{mn}}^5+\sum_{i=1}^{i=\mathrm{n}}\left(r_{\mathrm{mi}}^2t+2Br_{\mathrm{mi}}\frac{t^{-b+1}}{b-1}+B^2\frac{t^{-2b+1}}{-2b+1}\right)\Bigg|_{\tau_{\mathrm{mi}}}^{\tau_{\mathrm{mi-1}}}\right] \tag{10b}$$

where j represents the jth metastable AG domain.

Furthermore, the extended Maxwell model [43] is employed to formulate the constitutive stress-strain relationship, and the results are shown in Figure 2. Figure 2(a) illustrates the effects of mean-square displacement ($r(\tau)$) on the relaxation time of normal glass state, metastable glass state and rubbery state. As shown in Figure 2(b), the extend Maxwell model is incorporated of two branches in parallel, i.e., an equilibrium branch and a non-equilibrium one. A spring in the equilibrium branch represents the linear elastic behavior of rubbery state in the amorphous polymer. Whereas the non-equilibrium branch is used to describe the nonlinear viscoelastic behavior of dynamically metastable and normal glass states in the amorphous polymer, where there are three dashpots and one spring have been used to describe the metastable and normal AG glass transition domains, respectively.

Based on the above-mentioned Maxwell model, the constitutive stress-strain relationship can be expressed as,

$$\sigma+\tau\frac{\mathrm{d}\sigma}{\mathrm{d}t}=E_{\mathrm{eq}}\varepsilon+\left(E_{\mathrm{eq}}+E_{\mathrm{neq}}\right)\tau\frac{\mathrm{d}\varepsilon}{\mathrm{d}t},\ \left(\tau=\eta/E_{\mathrm{neq}}\right) \quad (11)$$

where σ and ε are the stress and strain of the polymer, and E_{eq} and E_{neq} are the moduli of the equilibrium and non-equilibrium branches, respectively.

Accordingly, the strain can be obtained as a function of stress for the amorphous polymer as,

$$\varepsilon=\frac{\sigma}{E_{\mathrm{eq}}}\left\{1-\exp\left[-\left(E_{\mathrm{eq}}E_{\mathrm{neq}}t\right)/\eta\left(E_{\mathrm{eq}}+E_{\mathrm{neq}}\right)\right]\right\} \quad (12)$$

(shape deformation)

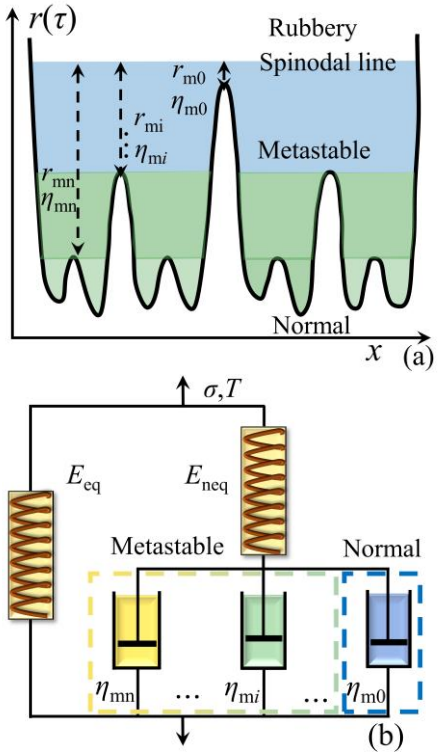

Figure 2 Schematic illustration of the extend Maxwell model. (a) Schematic illustration of mean-square displacements ($r(\tau)$) of normal glass state, metastable glass state and rubbery state; (b) The extend Maxwell model.

Figure 3 shows the analytical results of the strain (ε) as a function of relaxation time at different temperatures and stresses obtained using the equations (10) and (12). Parameters used in the equations (10) and (12) include E_{eq}=5 MPa, E_{neq}=1000 MPa [29], η=20 MPa·min, r_{mn}=1, τ_{mn}=1 min, ρ=-8.5 MPa·K, B=5.5 min, and b=0.6 [35,37,42]. For programming shape deformation of the amorphous Nafion SMP [34,40], the stored strain (ε_{s}) is gradually increased from 0 to 0.25 when the temperature is decreased from 413 K to 363 K at a constant stress (σ) of 2 MPa. Results show that the SMP takes 9 mins to achieve the relaxation of stored strain (ε_{s}) from 0.25 to 0.62, and the temperature is decreased from 363 K to 326 K at a constant stress (σ) of 3 MPa. Afterwards, the stored strain (ε_{s}) of SMP is increased from 0.62 to 1.58 at a constant stress (σ) of 5 MPa, and the temperature is decreased from 326 K to 296 K.

As another example for shape recovery of the amorphous Nafion SMP [34,40], a three-step shape recovery behavior is studied, i.e., the stored strain (ε_{s}) is gradually decreased in three steps, i.e., from 1.58 to 0.63 at 326 K, from 0.63 to 0.26 at 363 K, and from 0.26 to 0.01 at 413 K. The shape fixation ratio (R_{f}) and shape recovery ratio (R_{r}) can be calculated based on: $R_{\mathrm{f},i}$=100%×(ε_{sj}-$\varepsilon_{sj\text{-}1}$)/($\varepsilon_{\mathrm{load},j}$-$\varepsilon_{sj\text{-}1}$),and $R_{\mathrm{r},j}$=100%×(ε_{sj}-$\varepsilon_{\mathrm{recj}\text{-}1}$)/($\varepsilon_{sj}$-$\varepsilon_{sj\text{-}1}$) [34], where the jth pre-stored strain ($\varepsilon_{\mathrm{pre},j}$) is equal to ε_{sj} -$\varepsilon_{sj\text{-}1}$.

Effects of viscosity (η) and relaxation time (τ_{mn}) of the nth plateau on the shape deformation ratio and shape fixation behaviors for the amorphous SMP were analyzed using the proposed models based on equations (10a) and (12), and the obtained results are plotted in Figure 4. Parameters used in the equations (10a) and (12) include E_{eq}=10 MPa, E_{neq}=6000 MPa [29], σ=6 MPa, T=363 K, ρ=-10 MPa·K, r_{mn}=1, B=5.5 min, and b=0.6 [35,37,42]. As shown in Figure 4(a), the shape deformation ratio is decreased from 100%, 94.91%, 88.14%, 81.36% to 74.58%, with an increase in the viscosity (η) of amorphous SMP from 50 MPa·min, 75 MPa·min, 100 MPa·min, 125 MPa·min and 150 MPa·min, at the same relaxation time (τ_{mn}) of 20 min. These analytical results reveal that the shape deformation ratio is gradually decreased with an increase in the viscosity.

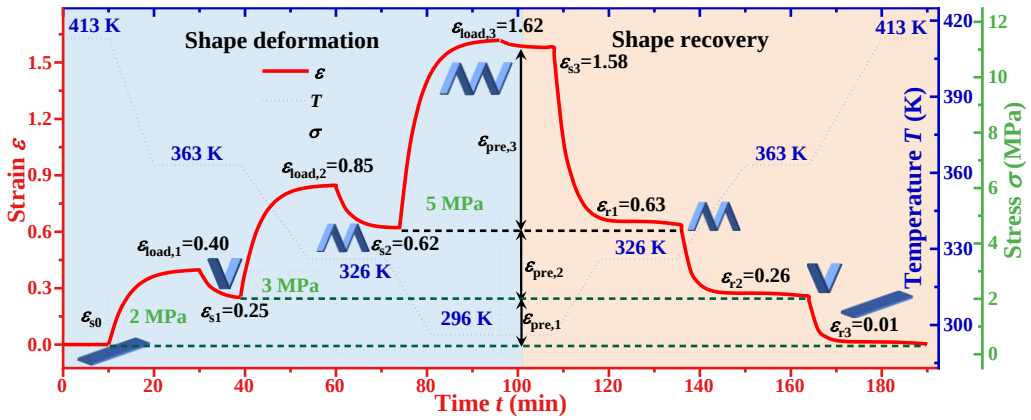

Figure 3 Shape deformation and recovery processes of the amorphous Nafion SMP [34,40] with the strain as a function of relaxation time.

On the other hand, Figure 4(b) shows the analytical results of recovery strains as a function of relaxation time. The shape fixity ratio (R_f) of the amorphous SMP is decreased from 77.97%, 74.58%, 69.49%, 64.41% to 54.24% with an increase in the relaxation time (τ_{mn}) from 1.91 min, 1.92 min, 1.93 min, 1.94 min to 1.95 min, at a constant deformation strain (ε_{load}) of 0.59. These analytical results reveal that a high mean-square displacement causes a low shape fixity ratio (R_f) for the SMP.

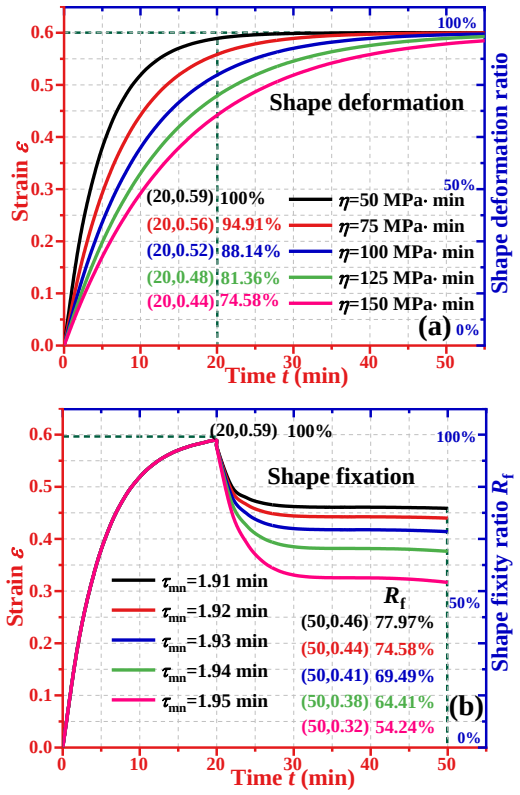

Figure 4 Analytical results of the strains as a function of relaxation time. (a) For shape deformation of SMP with η=50 MPa·min, 75 MPa·min, 100 MPa·min, 125 MPa·min and 150 MPa·min; (b) For shape fixity of SMP with τ_{mn}=1.91 min, 1.92 min, 1.93 min, 1.94 min and 1.95 min.

Furthermore, equation (10b) was used to predict the quadruple shape recovery behavior of the SMP in order to identify the effects of relaxation time (τ_{m3}) and mean-square displacement (r_{m3}) of the 3th plateau on the recovery strains. The obtained analytical results are plotted in Figure 5. Parameters used in the equation (10b) for calculations of stress-relaxation time include ρ=-8.5 MPa·K, r_{m2}=1, r_{m1}=1.13, r_{m0}=1.2, B=5.5 min and b=0.6 [35,37,42]. As shown in Figure 5(a), the SMP takes 83 min, 75 min, 63 min, 51 min and 27 min of relaxation time to complete their shape recovery, with an increase in relaxation time (τ_{m3}) from 1.91 min, 1.92 min, 1.93 min, 1.94 min to 1.95 min, in the first shape recovery process of the SMP at 326 K. Therefore, results shown in Figure 5(a) clearly reveal a triple-shape recovery behavior achieved.

On the other hand, Figure 5(b) shows the effect of mean-square displacement (r_{m3}) on recovery stains of the amorphous SMP. It is revealed that the SMPs take 8 min, 10 min, 22 min, 26 min and 30 min to complete their shape recoveries at a constant recovery ratio of 50%, whereas the mean-square displacements (r_{m3}) are $10^{-0.006}$, $10^{-0.004}$, $10^{-0.002}$, 1 and $10^{0.002}$. The relationships of relaxation time (τ_{m3}) and mean-square displacement (r_{m3}) are illustrated in Figure 5(c). With increases in both the relaxation time (τ_{m3}) and mean-square displacement (r_{m3}) of the 3th plateau, the SMP takes a longer relaxation time to complete the shape recovery, mainly resulted from the increase in viscosity and delayed relaxation of the AG domains.

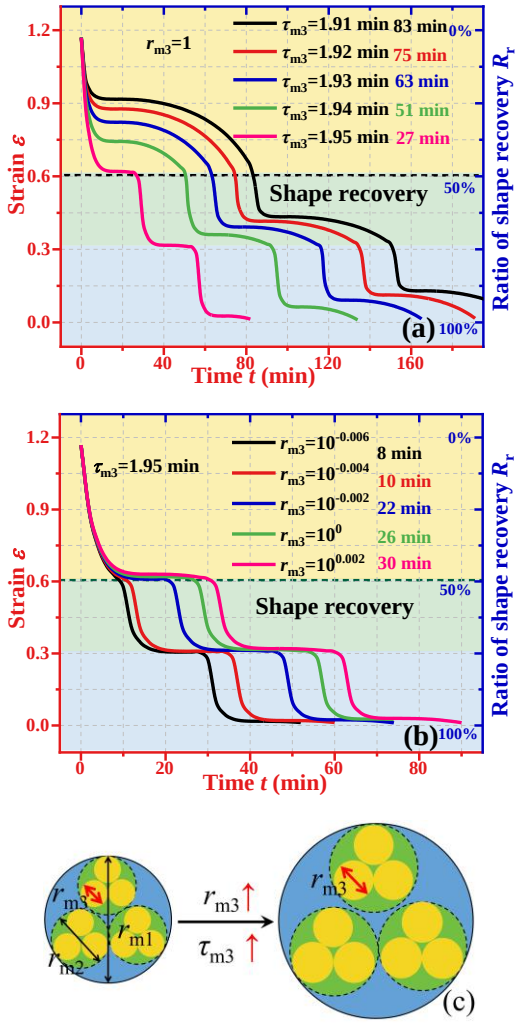

Figure 5 Effects of relaxation time (τ_{m3}) and mean-square displacement (r_{m3}) of the 3th plateau on the recovery behavior of SMP. (a) Effect of relaxation time (τ_{m3}); (b) Effect of mean-square displacement (r_{m3}); (c) Schematic illustrations of working principles of relaxation time (τ_{m3}) and mean-square displacement (r_{m3}) in metastable AG domain.

3 Experimental verifications of SMP undergoing multi-SME

Experimental data reported in Ref. [34,40] for the Nafion

SMP were used to verify the analytical results obtained using our newly proposed model. The experimental conditions are listed as follows. During the shape deformation, uniaxial tension measurements were conducted using the Nafion SMP at a cooling rate of 5 K/min, while the externally mechanical force was removed during the shape fixation/recovery at both a cooling and heating rate of 5 K/min. The stress curves were plotted as a function of temperature as shown in Figures 6, 7 and 8.

To verify the newly proposed model based on equations of (10) and (12), the reported experimental data [34] for amorphous Nafion SMP with a dual-SME have been employed to compare with the analytical results obtained using the proposed model. All the values of parameters used in equations (10) and (12) are listed as follows: E_{eq}=0.5 MPa, E_{neq}=900 MPa [34], σ=2.3 MPa, η=1.5 MP·min, T=333.15 K, ρ=-8.5 MPa·K, r_{mn}=0.918, τ_{mn}=1.94 min, B=5.5 min, and b=0.6 [35,37,42].

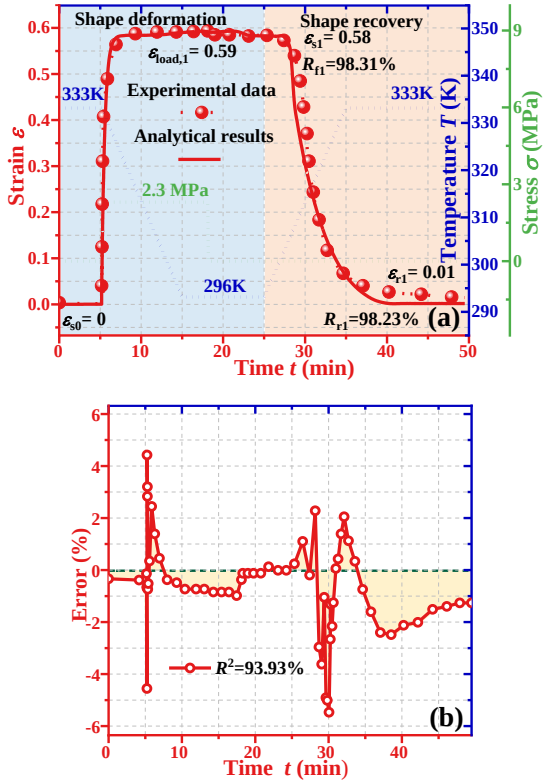

Figure 6 Comparisons of analytical results of equations (10) and (12) and the experimental data [34] of Nafion SMP with dual-SME. (a) For the strain-relaxation time curves; (b) Error of analytical and experimental results.

Figure 6 shows both the analytical and experimental results, which are in well agreements. As shown in Figure 6(a), the deformed strain (ε_{load}) of the Nafion SMP (with T_g of 293 K) when cooled down from 333 K to 293 K, was increased from 0 to 0.59 under the external stress of 2.3 MPa. Results show that the Nafion SMP has a shape fixation ratio (R_f) of 98.31%. For programming shape recovery, the stored strain (ε_s) of this SMP is gradually released from 0.58 to 0.01 with an increase in temperature from 293 K to 333 K, resulting in a shape recovery ratio (R_r) of 98.23%. The divergences between the analytical and experimental results were calculated, and the correlation index (R^2) is 93.93% as shown in Figure 6(b). These results indicate that the proposed model can be applicable to predict the experimental results for the Nafion SMP with dual-SME, where the error is limited to ±5%.

Equations (10) and (12) have been further used to predict the triple-SME of the Nafion SMP. The calculation results were further compared with the experimental data reported in Ref. [34,40], both of which are plotted in Figure 7. All the values of parameters used in the calculation based on these equations are listed in Table 1, and ρ=-8.5 MPa·K, B=5.5 min, and b=0.6 [35,37,42]. As shown in Figure 7(a), a clear two-stage shape recovery for the Nafion SMP with a triple-SME (e.g., the first stage of transition is originated from the decrease in recovery strain (ε_{r1}) from 1.05 to 0.43 at 326 K, while the second one is due to the decrease in recovery strain (ε_{r2}) from 0.43 to 0.04 at 413 K) has been well predicted using the equations (10) and (12).

The thermomechanical process of shape deformation is defined as follows. The Nafion SMP was firstly deformed under a stress load of 0.35 MPa and strain of 0.49, resulting in a stored strain (ε_{s1}) of 0.42 and a shape fixity ratio (R_{f1}) of 85.71%. Then the SMP was deformed under an external stress of 4.35 MPa and strain of 1.07, resulting into a stored strain (ε_{s2}) of 1.05 and shape fixity ratio (R_{f2}) of 94.03%. The divergences between the analytical and experimental results [34] were calculated based on their correlation index (R^2), and the obtained data is 98.72%.

Table 1. Values of parameters used in equations (10) and (12) for Nafion SMP [34,40].

Nafion	Shape deformation			Shape fixation	Shape recovery	
Stage	E_{eq}(MPa)	E_{neq}(MPa)	η(MPa·min)	r_{mn}	τ_{mn} (min)	r_{mn}
1	1.3	900	1.5	1.62	1.94	0.97
2	3.84			1.63		0.93
1	0.71	900	1.3	0.97	1.94	0.97
2	6.64		2.6	0.91		0.93

As shown in Figure 7(b), another two-stage shape recovery of Nafion SMP with a triple-SME (e.g., the first stage of transition is originated from the decrease in recovery strain (ε_{r1}) from 0.92 to 0.26 at 333 K, while the second one is due to the decrease in recovery strain (ε_{r2}) from 0.26 to 0.01 at 373 K) was predicted using the constitutive model, where the SMP was undergone a different thermomechanical process. In this case, the shape deformation of this SMP was programmed as follows. The Nafion SMP was firstly deformed under a stress load of 0.8 MPa and strain of 0.44, resulting in a stored strain (ε_{s1}) of 0.25 and a shape fixity

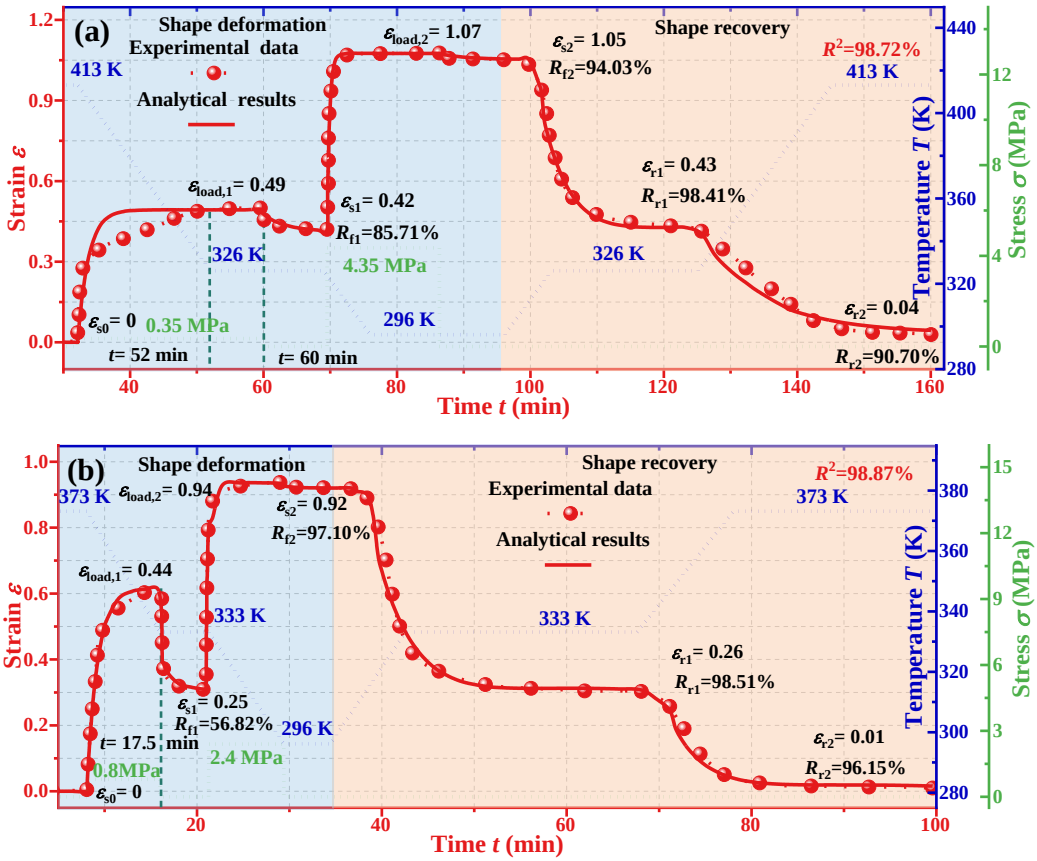

Figure 7 Comparisons of analytical results of equations (10) and (12) and experimental data of Nafion SMP [34,40]. (a) For the strain-relaxation time curves of the Nafion SMP with triple-SME [34]. (b) For the strain- relaxation time curves of the Nafion SMP with triple-SME [40].

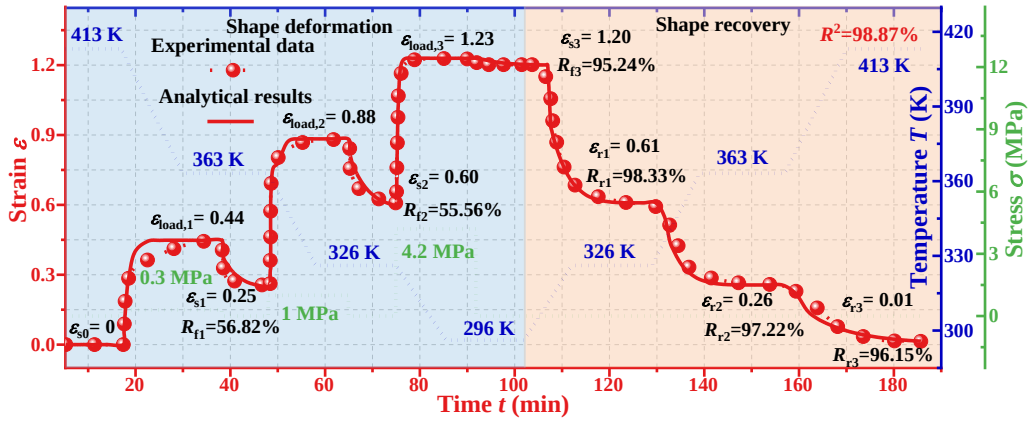

Figure 8 Comparisons of analytical results of equations (10) and (12) and experimental data of Nafion [34] for the strain-relaxation time curves of the Nafion SMP with quadruple-SME.

ratio (R_{f1}) of 56.82%. Then the SMP was deformed under a stress load of 2.4 MPa and strain of 0.94, resulting into a stored strain (ε_{s2}) of 0.92 and a shape fixity ratio (R_{f2}) of 97.10%. The divergences between the analytical and experimental results [40] were assessed based on their correlation index (R^2), which is 98.87%. This shows that the analytical results of the proposed model agree well with the experimental data of Nafion SMP with various thermomechanical histories [34,40].

To further verify the model, experimental data [34] of another group of Nafion SMP showing a quadruple-SME have been employed to compare with those analytical results obtained using the proposed model based on the equations of (10) and (12). All the parameters used in the equations are listed in Table 2, where ρ=-8.5 MPa·K, B=5.5 min, and b=0.6 [35,37,42]. In the shape deformation process, the strain of Nafion SMP is increased from 0 to 0.44 under the stress load of 0.3 MPa, when the temperature is decreased

from 413.15 K to the 363.15 K, as shown in Figure 8.

Table 2. Values of parameters used in equations (10) and (12) for Nafion SMP [34].

Nafion	Shape deformation			Shape fixation	Shape recovery	
Stage	E_{eq} (MPa)	E_{neq} (MPa)	η (MPa·min)	r_{mn}	τ_{mn} (min)	r_{mn}
1	0.67		0.8	0.96		0.94
2	1.61	900	1.5	0.93	1.94	0.95
3	6.76		2.1	0.91		0.93

The obtained stored strain (ε_{s1}) is 0.25 and the shape fixity ratio (R_{f1}) is 56.82%. Moreover, the strain of Nafion SMP is increased from 0.25 to 0.88 under the stress load of 1.0 MPa, with a decrease in temperature from 363.15 K to 326.15 K, resulting in a stored strain (ε_{s2}) of 0.60 and a shape fixity ratio (R_{f2}) of 55.56%. Furthermore, the strain of Nafion SMP is increased from 0.60 to 1.23 under the stress load of 4.2 MPa, with a decrease in temperature from 326.15 K to 293.15 K, resulting in a stored strain (ε_{s3}) of 1.20 and a shape fixity ratio (R_{f3}) of 95.24%. Following the thermomechanical processes of SMPs, a three-stage shape recovery of Nafion SMP with a quadruple-SME are achieved, and the experimental data have also well been predicted using the constitutive model. The details of shape recovery processes are given as follows. The first stage of transition is originated from the decrease in recovery strain (ε_{r1}) from 1.20 to 0.61 at 326.15 K. The second one is due to the decrease in recovery strain (ε_{r2}) from 0.61 to 0.26 at 363.15 K. Then the third one is resulted from the decrease in recovery strain (ε_{r3}) from 0.26 to 0.01 at 413.15 K. Whereas the shape recovery ratios of these three transitions are R_{r1}=98.33%, R_{r2}=97.22% and R_{r3}=96.15%, respectively. Finally, the correlation index (R^2) between the analytical and experimental results [34] were calculated to be 98.87% for the Nafion SMP with a quadruple-SME, indicating that good agreements between analytical results and experimental data have been achieved.

4 Conclusions

In this study, a spinodal dynamic model of metastable glass transition is established to investigate the working principle of thermomechanical process in multi-SME of the amorphous SMPs. Mean-square displacement of metastable AG domains plays an essential role in linking dynamic glass transitions to multiple shape recovery behaviors of the amorphous SMP. Then a dynamically spinodal model is developed to understand the effect of thermomechanical process on the dynamic glass transition, based on the statistic viscosity equation and phase transition model. Furthermore, effect of thermomechanical process on shape recovery behavior has been investigated using the relaxation time function in the SMP, in terms of mean-square displacement, temperature, heating/cooling rate, stress load, shape deformation ratio and shape recovery ratio. Finally, the proposed model is able to predict the dual-, tripe- and quadruple-SME in amorphous SMP undergoing multiple shape recovery behaviors and verified using the experimental results of Nafion SMP reported in the literature. This newly developed model provides an in-depth insight into the spinodal model in the dynamic nonequilibrium of glass transition, which governs the SME and shape recovery behavior of the amorphous SMPs.

This work was financially supported by the National Natural Science Foundation of China (Grant Nos. 11725208, 12172107), and International Exchange Grant (Grant No. 201078).

1 Herath M, Epaarachchi J, Islam M, et al. Light activated shape memory polymers and composites: a review. Eur Polym J, 2020, 136**:** 109912
2 Zhao F, Shi Y, Pan L J, et al. Multifunctional nanostructured conductive polymer gels: synthesis, properties, and applications. Accounts Chem Res, 2017, 50: 1734–1743
3 Chortos A, Liu J, Bao Z A. Pursuing prosthetic electronic skin. Nat Mater, 2016, 15: 937–950
4 Darabi M A, Khosrozadeh A, Mbeleck R, et al. Skin-inspired multifunctional autonomic-intrinsic conductive self-healing hydrogels with pressure sensitivity, stretchability, and 3D printability. Adv Mater, 2018, 30: 1705922
5 Kim S H, Jung S, Yoon I S, et al. Ultrastretchable conductor fabricated on skin-like hydrogel-elastomer hybrid substrates for skin electronics. Adv Mater, 2018, 30: 1800109
6 Xia Y L, He Y, Zhang F H, et al. A review of shape memory polymers and composites: mechanisms, materials, and applications. Adv Mater, 2020, 33: 2000713
7 Wei Z, Yang J H, Liu Z Q, et al. Novel Biocompatible Polysaccharide-Based Self-Healing Hydrogel. Adv Funct Mater, 2015, 25: 1352–1359
8 Xiao R, Huang W M. Heating/solvent responsive shape-memory polymers for implant biomedical devices in minimally invasive surgery: current status and challenge. Macromol Biosci, 2020, 20: 2000108
9 Buffington S L, Paul J E, Ali M, et al. Henderson J H Enzymatically triggered shape memory polymers. Acta Biomater, 2018, 84: 88–97
10 Liu J Y, Lu H B, Fu Y Q. Yielding mechanisms for mechano-chemo-thermal couplings in amorphous shape memory polymer undergoing molecular entanglement. J Phys D Appl Phys, 2021, 54: 415302
11 Ramdas M R, Kumar K S S, Nair C P R. Heat and solvent responsive polytriazole: shape recovery properties in different solvents. RSC Adv, 2016, 6: 53602–13
12 Lu H B, Liu Y J, Leng J S, et al. Qualitative separation of the effect of the solubility parameter on the recovery behavior of shape-memory polymer Smart Mater Struct, 2009, 18: 085003
13 Ji S B, Fan F Q, Sun C X, et al. Visible light-induced plasticity of shape memory polymers. ACS Appl Mater Inter, 2017, 9: 3169–3175
14 Wang X D, Jian W, Lu H B, et al. Selective entanglement coupling of nanoparticles in polymer nanocomposite with high shape recovery stress. Compos Sci Technol, 2021, 207: 108728
15 Wang X D, Jian W, Lu H B, et al. Modeling Strategy for Enhanced Recovery Strength and a Tailorable Shape Transition Behavior in Shape Memory Copolymers. Macromolecules, 2019, 52: 6045–6054
16 Meng Q H, Hu J L. A review of shape memory polymer composites and blends Composites: Part A, 2009, 40: 1661–1672

17 Chen H M, Wang L, Zhou S B. Recent progress in shape memory polymers for biomedical applications. Chinese J Polym Sci, 2018, 36: 905–917
18 Delaey J, Dubruel P, Van Vlierberghe S. Shape-memory polymers for biomedical applications. Adv Funct Mater, 2020, 30: 1909047
19 Lendlein A, Langer R. Biodegradable, elastic shape-memory polymers for potential biomedical applications. Science, 2002, 296: 1673–1676
20 Li Y J, Zhang F H, Liu Y J, et al. 4D printed shape memory polymers and their structures for biomedical applications. Sci China Tech Sci, 2020, 63: 545–560
21 Lin C, Zhang L J, Liu Y J, et al. 4D printing of personalized shape memory polymer vascular stents with negative Poisson's ratio structure: A preliminary study. Sci China Tech Sci, 2020, 63: 578–588
22 Zhang Y F, Zhang N B, Hingorani H, et al. Fast-response, stiffness-tunable soft actuator by hybrid multimaterial 3D printing. Adv Funct Mater, 2019, 29: 1806698
23 Ma S Q, Zhang Y P, Wang M, et al. Recent progress in 4D printing of stimuli-responsive polymeric materials. Sci China Tech Sci, 2020, 63: 532–544
24 Wang S, Brigham J C. A computational framework for the optimal design of morphing processes in locally activated smart material structures. Smart Mater Struct, 2012, 21: 105016
25 Santo L, Quadrini F, Squeo E A, et al. Behavior of shape memory epoxy foams in microgravity: experimental results of STS-134 mission. Microgravity Sci Technol, 2012, 24: 287–296
26 Lan X, Liu L W, Zhang F H, et al. World's first spaceflight on-orbit demonstration of a flexible solar array system based on shape memory polymer composites. Sci China Tech Sci, 2020, 63: 1436–1451
27 Cohen M H, Turnbull D. Molecular transport in liquids and glasses. J Chem Phys, 1959, 31: 1164–1169
28 Schweizer K S, Saltzman E J. Theory of dynamic barriers, activated hopping, and the glass transition in polymer melts. J Chem Phys, 2004, 121: 1984–2000
29 Liu J Y, Gorbacheva G, Lu H B, et al. Dynamic equilibria with glass transition heterogeneity and tailorable mechanics in amorphous shape memory polymers. Smart Mater Struct, 2022, 31: 075022
30 Liu J Y, Xing Z Y, Lu H B, et al. Interfacial confinement in semi-crystalline shape memory polymer towards sequentially dynamic relaxations. Int J Appl Mech, 2021, 13: 2150117
31 Li Y X, Hu J Y, Liu Z S. A constitutive model of shape memory polymers based on glass transition and the concept of frozen strain release rate. Int J Solids Struct, 2017, 124: 252–263
32 Nguyen T D, Yakacki C M, Brahmbhatt P D, et al. Modeling the relaxation mechanisms of amorphous shape memory polymers. Adv Mater, 2010, 22: 3411–3423
33 Yu K, Xie T, Leng J S, et al. Mechanisms of multi-shape memory effects and associated energy release in shape memory polymers. Soft Matter, 2012, 8: 5687–5695
34 Xie T. Tunable polymer multi-shape memory effect. Nature, 2010, 464: 267–270
35 Charbonneau P , Kurchan J, Parisi G, et al. Glass and jamming transitions: from exact results to finite-dimensional descriptions. Annu Rev Conden Ma P, 2018, 8: 265–288
36 Adam G, Gibbs J H. On the temperature dependence of cooperative relaxation properties in glass-forming liquids. J Chem Phys, 1965, 43: 139–146
37 Gotze W. Complex dynamics of glass-forming liquids: A mode-coupling theory. Oxford University Press, Oxford, 2008
38 De Gennes P G. Scaling concepts in polymer physics. Cornell University Press, New York, 1979
39 Liu Y P, Gall K, Dunn M L, et al. Thermomechanics of shape memory polymers: uniaxial experiments and constitutive modeling. Int J Plast, 2006, 22: 279–313
40 Li J J, Xie T. Significant impact of thermo-mechanical conditions on polymer triple-shape memory effect. Macromolecules, 2011, 44: 175–180
41 Charbonneau P, Kurchan J, Parisi G, et al. Fractal free energy landscapes in structural glasses. Nat Commun, 2014, 5: 3725
42 Maimbourg T, Kurchan J, Zamponi F. Solution of the dynamics of liquids in the large-dimensional limit. Phys Rev Lett, 2016, 116: 015902
43 Treloar L R G. The physics of rubber elasticity. Oxford University Press, Oxford, 2005